Unexpected Halogen-Induced Electron-Phonon Superconductivity in Two-dimensional Materials

L.-B. MENG,* S. Ni, W. M. ZHOU

Supplementary Information

I. Computational details.

The superconducting transition temperature T_c was estimated by using the modified approximate McMillan equation [1],

$$k_B T_c = \frac{\hbar\omega_{\log}}{1.2}\exp\left(\frac{-1.04(1+\lambda)}{\lambda-\mu^*-0.62\lambda\mu^*}\right) \quad (1)$$

where λ is the EPC strength and the prefactor $\omega_{\log}$ is a properly defined logarithmic average frequency suggested by Allen and Dynes [2], while μ^* is a parameter, accounting for the effective Coulomb repulsion.

The total EPC strength λ can be calculated either by the summation of the individual EPC coefficient $\lambda_{\mathbf{q}\nu}$ in the full Brillouin zone (BZ) for all phonon modes or by the integral of the Eliashberg spectral function $\alpha^2F(\omega)$[3], as

$$\lambda = \sum_{\mathbf{q}\nu}\lambda_{\mathbf{q}\nu} = 2\int_0^\infty \frac{\alpha^2F(\omega)}{\omega}d\omega \ . \quad (2)$$

The individual EPC coefficient $\lambda_{\mathbf{q}\nu}$ for the νth phonon mode at the wave-vector $\mathbf{q}$ is defined as

$$\lambda_{\mathbf{q}\nu} = \frac{1}{N(E_\mathrm{F})M\omega_{\mathbf{q}\nu}^2}\int_{\mathrm{BZ}}\frac{d\mathbf{k}}{\Omega_{\mathrm{BZ}}}\sum_{ij}\delta\left(E_{i,\mathbf{k}}-E_\mathrm{F}\right) \times \delta\left(E_{j,\mathbf{k+q}}-E_\mathrm{F}\right)\left|\left\langle\psi_{i,\mathbf{k}}\middle|\epsilon_{\mathbf{q}\nu}\cdot\nabla V\middle|\psi_{j,\mathbf{k+q}}\right\rangle\right|^2 \quad (3)$$

and the Eliashberg spectral function $\alpha^2F(\omega)$ is given by

$$\alpha^2F(\omega) = \frac{1}{2}\sum_\nu\int_{\mathrm{BZ}}\frac{d\mathbf{q}}{\Omega_{\mathrm{BZ}}}\lambda_{\mathbf{q}\nu}\omega_{\mathbf{q}\nu}\delta\left(\omega-\omega_{\mathbf{q}\nu}\right) \quad (4)$$

The logarithmically averaged characteristic phonon frequency $\omega_{\log}$ is defined as

$$\omega_{\log} = \exp\left[\frac{2}{\lambda}\int_0^\infty \alpha^2F(\omega)\frac{\ln\omega}{\omega}d\omega\right] \ . \quad (5)$$

The first-principle atomic crystal structure calculations were preformed based on density functional theory (DFT) within the projector augmented wave (PAW) [4] pseudopotential method and Perdew-Burke-Ernzerhof (PBE) functional [5] as implemented in the Vienna ab initio simulation package (VASP) [6]. A plane-wave cutoff energy of 600 eV and 17 × 17 × 1 Monkhorst-Pack *k*-point were employed; To eliminate interactions between adjacent layers, a large vacuum distance of 20 Å along

the perpendicular direction was used; All structures were fully relaxed until the residual forces on each atom were less than 10^{-4} eV/Å.

The electronic structures, lattice dynamics and EPC calculations were performed by employing the local density approximation and norm-conserving pseudo-potentials as implemented in the Quantum-ESPRESSO (QE) package [7]. The kinetic energy cutoff and the charge density cutoff of the plane wave basis are chosen to be 110 and 440 Ry, respectively. Self-consistent electron density is evaluated by employing a 36 × 36 × 1 **k**-mesh; Both phonon and EPC are calculated within density functional perturbation theory (DFPT) by using a 12 × 12 × 1 **q**-mesh. The convergence of phonon dispersion and EPC with respect to the energy cutoff and q-point sampling has been carefully checked. Phonon frequencies are converged within 3 cm^{-1} and T_c are converged within 1 K (see Table S1). First-principles molecular dynamics (FPMD) simulations in VASP under constant temperature and volume (NVT) were performed with the temperature controlled by a Nose-Hoover thermostat [8] to check the thermal stability. A relatively large supercell of 6 × 6 × 1 was adopted and each simulation lasted for 8 picosecond (ps) with a time step of 2 femtosecond (fs).

Table S1: Convergence testing for the characteristic vibrational mode E_{2g} (in cm^{-1}), EPC λ, logarithmically averaged phonon frequency ω_{log} (in Kelvin), and critical transition temperature T_c (in Kelvin) versus different **k** and **q** meshes.

System	**k**, **q**-mesh settings in QE	E_{2g}	λ	ω_{log}	T_c
ML MgB_2	**k**=64×64×1,32×32×1,**q**=8×8×1	615.2	0.58	566.4	19.0
	k=72×72×1,36×36×1,**q**=12×12×1	617.7	0.61	534.9	20.0
F-MgB_2	**k**=64×64×1,32×32×1,**q**=8×8×1	595.0	1.65	332.5	46.8
	k=72×72×1,36×36×1,**q**=12×12×1	597.7	1.35	389.4	46.4
Cl-MgB_2	**k**=64×64×1,32×32×1,**q**=8×8×1	404.2	1.14	458.8	46.1
	k=72×72×1,36×36×1,**q**=12×12	405.0	1.16	448.8	46.2

To verify the reliability of our computational methods and gain the effective Coulomb repulsion μ^* in the T_c prediction, the crystal structure, electronic, vibrational, and superconducting properties of the parent bulk MgB_2 were calculated as the benchmark. In this calibrating computation, the crystal lattice was relaxed by a 17 × 17 × 15 Monkhorst-Pack **k**-point and phonon and EPC are calculated with an 8 × 8 × 6 **q**-mesh, and other settings are same as that of 2D systems described above. The obtained results were listed in Table 1 and shown in Fig. S1. The calculated lattices of a = 3.077 Å and c = 3.512 Å are well consistent with the experimental measurements (a_{exp} = 3.086 Å and c_{exp} = 3.524 Å) [9]. The

obtained electronic structure, phonon dispersion and EPC are consistent with the results of previous works [10,11]. When with the retarded Coulomb parameter $\mu^* = 0.05$, the calculated EPC λ and T_c are 0.76 and 40 K, respectively, which both well reproduce the experimental results of $\lambda_{exp} \sim 0.75$ and $T_c \sim 39.2$─40.2 K [12]. With the structural similarity, we thus reasonably select $\mu^* = 0.05$ in the estimation of superconductivity for all herein studied systems.

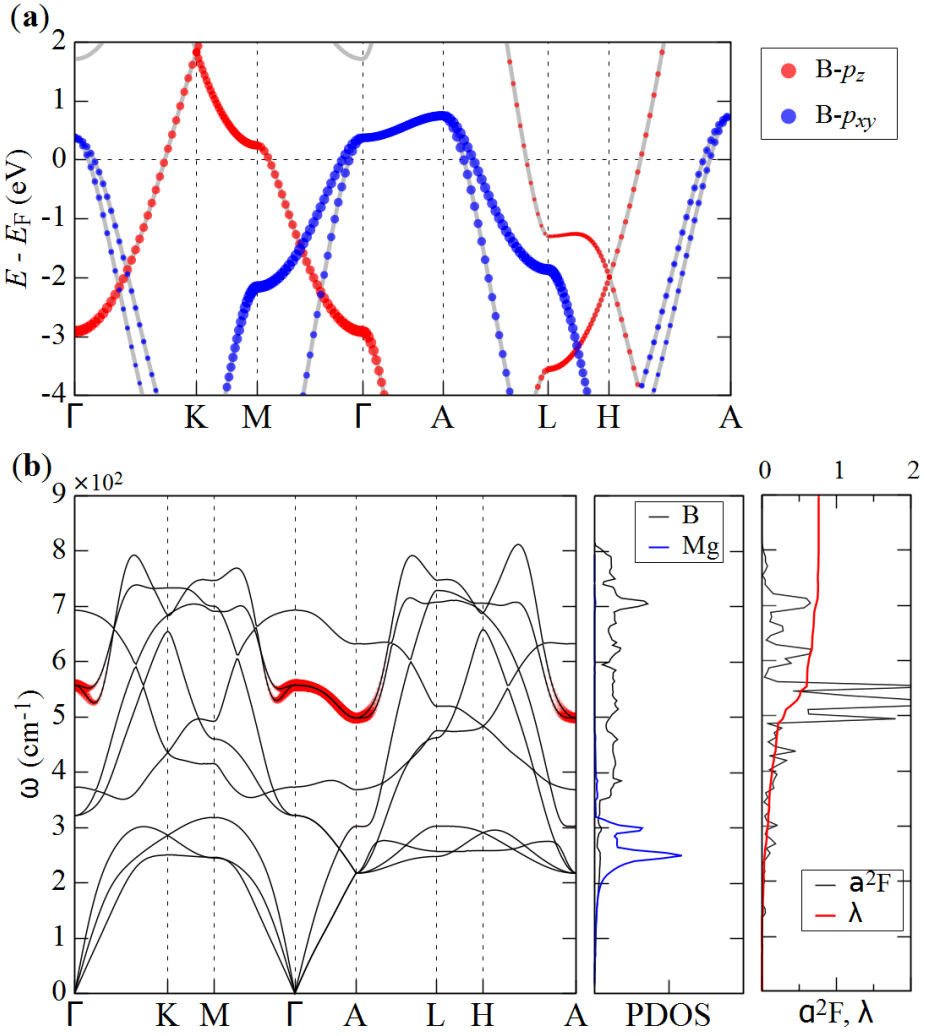

FIG. S1. (a) Electronic band structure decorated with atomic orbital resolved contributions (color encoded dots) for bulk MgB_2. (b) phonon dispersion curve decorated with individual λ_{qv} strength (red dots), atom-resolved phonon density of states (PDOS), and Eliashberg function $\alpha^2F(\omega)$ and frequency-dependence $\lambda(\omega)$.

II. Supplementary Data and Figures

Table S2: Superconducting transition temperature (T_c, in Kelvin) estimated with different Coulomb parameter (μ*).

System	T_c (μ*=0.05)	T_c (μ*=0.10)	T_c (μ*=0.13)
F-MgB_2	46.4	40.5	36.5
Cl-MgB_2	46.2	38.9	34.4
F-TiB_2	17.3	14.2	11.3
Cl-TiB_2	20.0	17.3	14.4

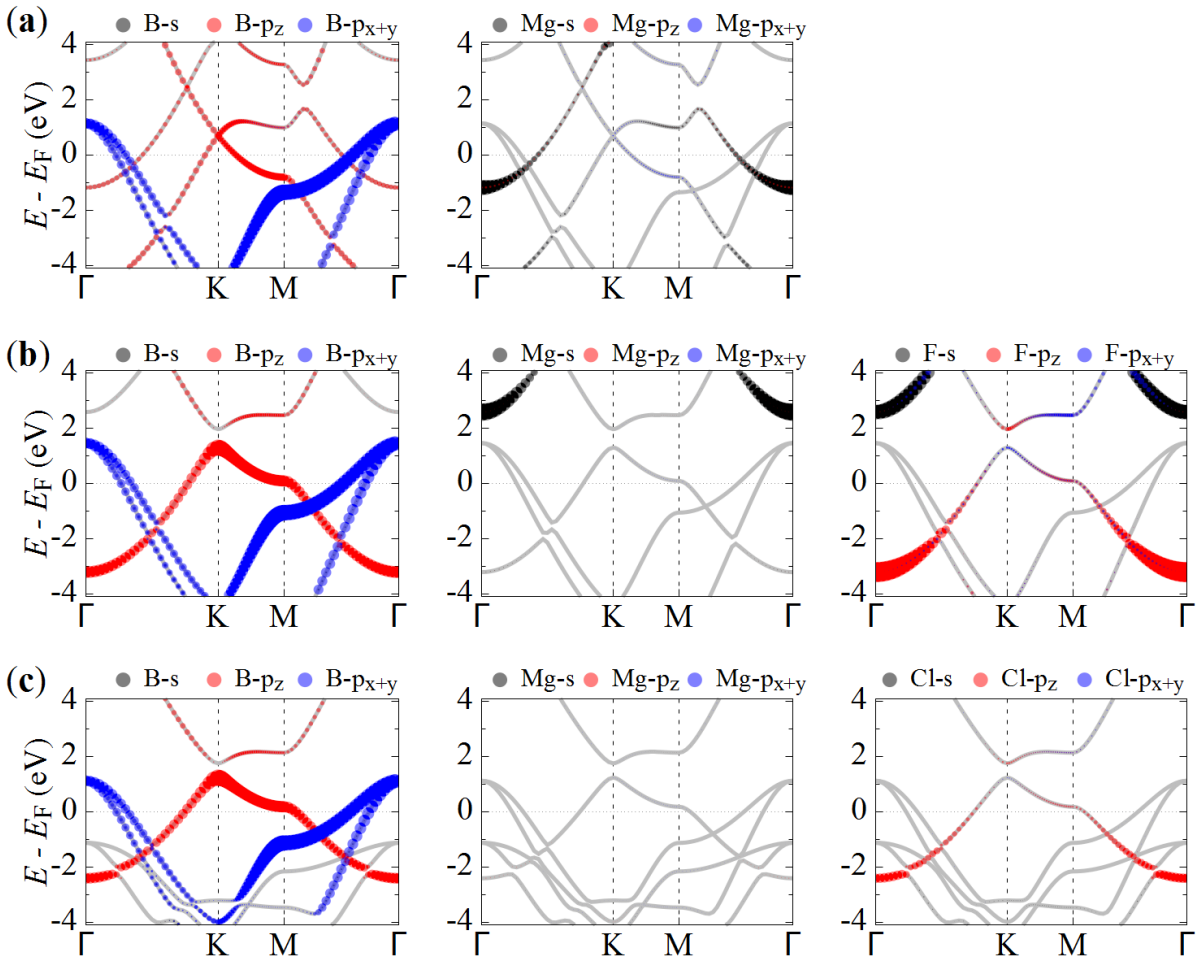

FIG. S2. Electronic band structure decorated with atomic orbital resolved contributions (color encoded dots) for (a) ML MgB_2, (b) F-MgB_2 and (c) Cl-MgB_2. The size of F-p_z dots has been amplified 4-fold for clarity in (b).

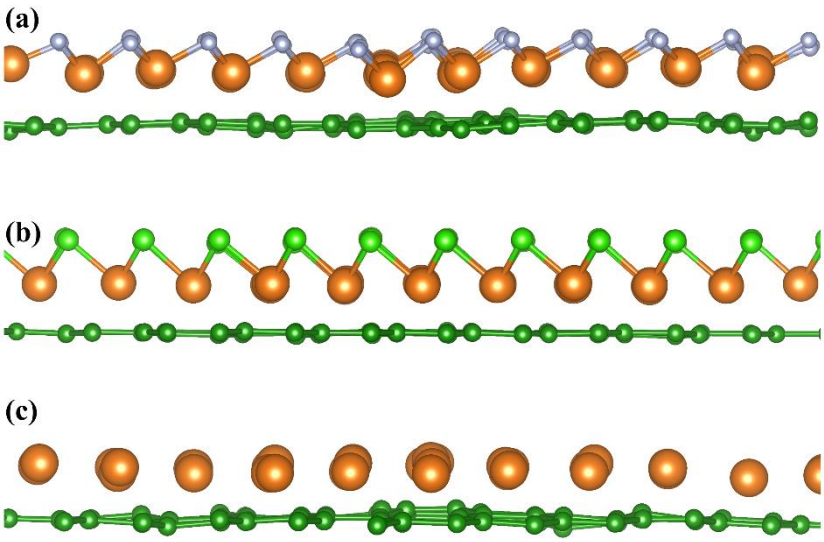

FIG. S3. Side views of final structure snapshots of 8 ps FPMD simulations for (a) F-MgB_2 at 200 K, (b) Cl-MgB_2 at 80 K, and (c) 2D MgB_2 at 350 K. Structures may collapse at respectively higher temperatures.

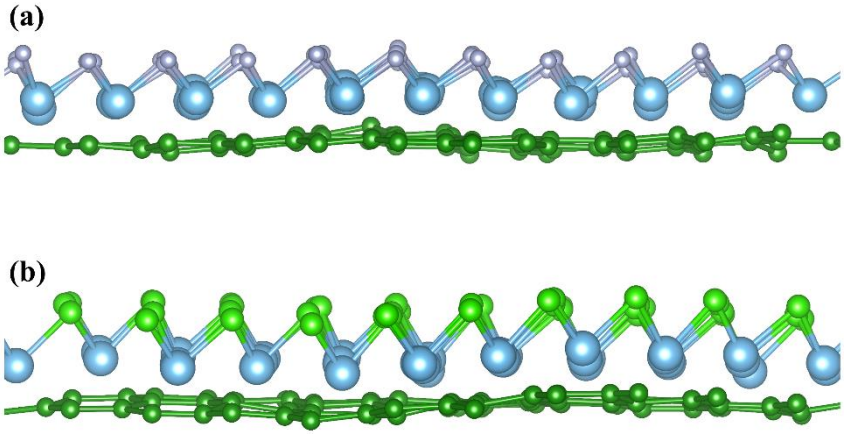

FIG. S4. Side views of final structure snapshots of 8 ps FPMD simulations at 500 K for (a) F-TiB_2 and (b) Cl-TiB_2.

NOTE: Snapshots of the geometries at the end of 8 ps FPMD simulations indicate that fluorinated/chlorinated TiB_2 can well maintain its structural integrity up to 500 K (only with the expected thermal oscillations of the atoms around their equilibrium positions); the F/Cl-MgB_2 has a lower thermal stability and may collapse at room temperature due to the weakness of Mg-B bond (relative to the Ti-B bond), while the isolated MgB_2 monolayer can be thermally stable at 350 K. These MD results suggest that low temperature are required for the synthesis and store for the fluorinated/chlorinated MgB_2 systems.

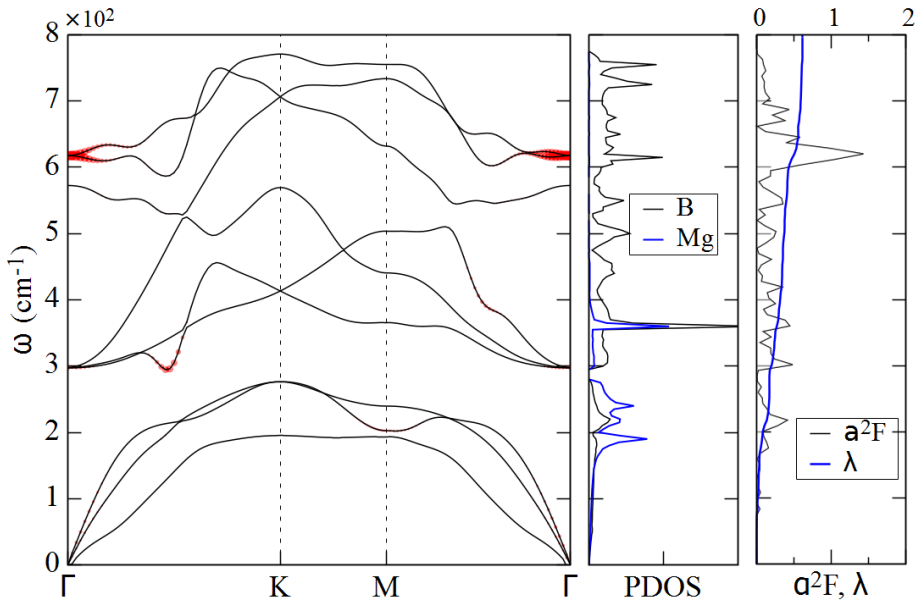

FIG. S5. Phonon dispersion curve decorated with individual $\lambda_{\mathbf{q}\nu}$ strength (red dots), atom-resolved phonon density of states (PDOS), and Eliashberg function $\alpha^2F(\omega)$ and frequency-dependence $\lambda(\omega)$ of ML MgB_2.

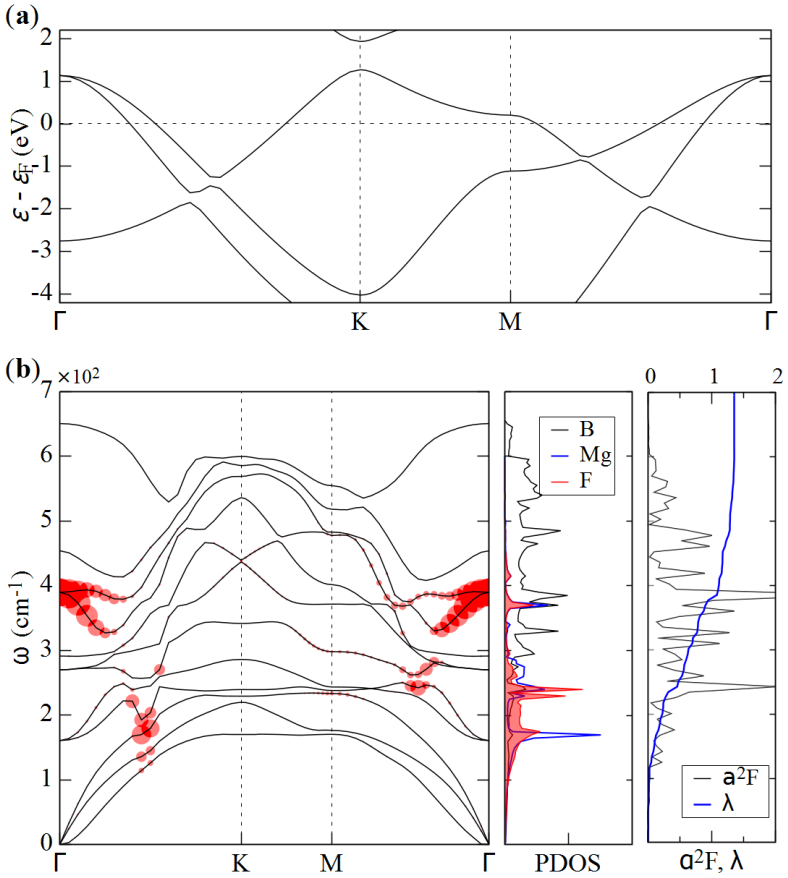

Figure S6. (a) Electronic band structure, and (b) phonon dispersion curve (left panel), atom-resolved phonon density of states (PDOS, mid panel), and Eliashberg function $\alpha^2F(\omega)$ and $\lambda(\omega)$ (right panel) of F-MgB_2 under δ = 5% tensile strain. The color dots decorated in phonon dispersion indicate the strength of individual EPC $\lambda_{\mathbf{q}\nu}$.

NOTE: The tensile strain mainly affects the vibrational states and resulting EPC modes. The original remarkable Kohn anomaly in the acoustic branches is removed, and the most significant $\lambda_{\mathbf{q}\nu}$ are distributing around the high-frequency optical E_{2g} mode near the Γ point (with E_{2g} frequency much declining). It leads to an increase of the logarithmic average frequency ω_{log} (389.6 K → 423.7 K), while the total EPC strength λ does almost not change ($\lambda \sim 1.35$).

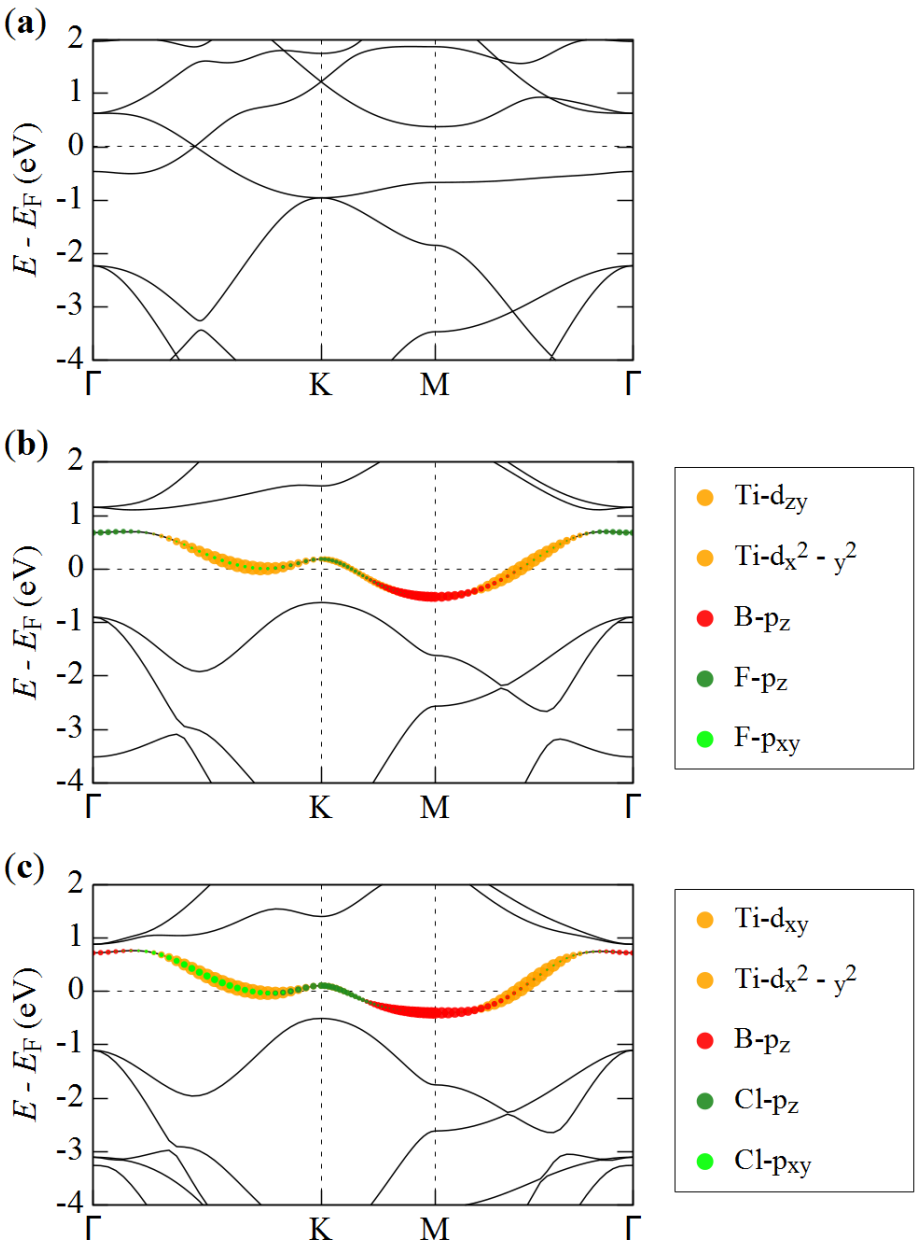

Figure S7. Electronic band structures of (a) ML TiB_2, (b) F-TiB_2 and (c) Cl-TiB_2. The decorating color dots indicate the atomic-orbital resolved contributions. The sizes of F-p_z and Cl-p_z dots have been amplified four-fold for clarity in (b,c).

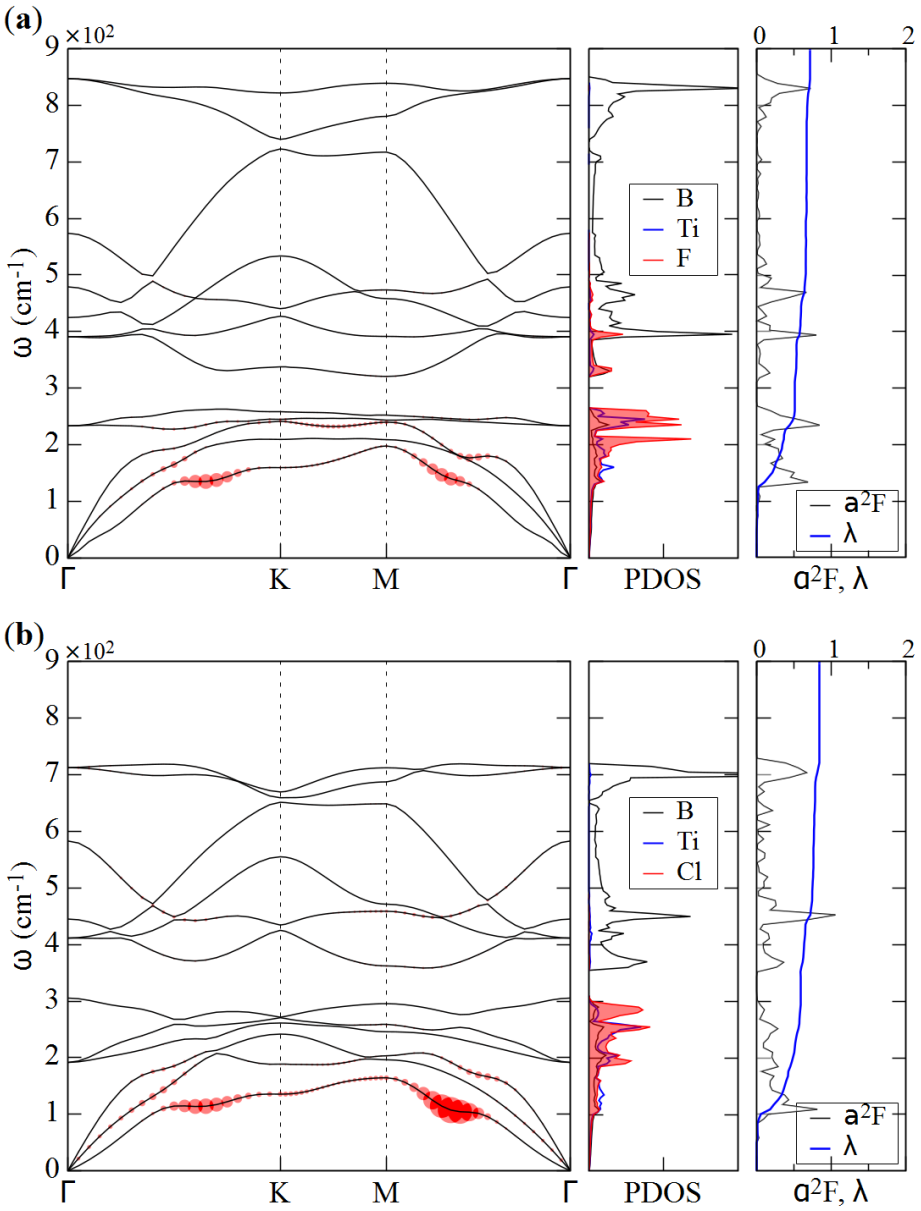

Figure S8. Phonon dispersion curve (left panel), atom-resolved phonon density of states (PDOS, mid panel), and Eliashberg function $\alpha^2F(\omega)$ and $\lambda(\omega)$ (right panel) of (a) F-MgB_2 and (b) Cl-MgB_2. The color dots decorated in phonon dispersion indicate the strength of individual $\lambda_{\mathbf{q}\nu}$.

References

[1] W. L. McMillan, Phys. Rev. 167, 331 (1968).

[2] P. B. Allen and R. C. Dynes, Phys. Rev. B 12, 905 (1975).

[3] G. M. Eliashberg, Sov. Phys. JETP 11, 696 (1960).

[4] P. E. Blochl, Phys. Rev. B 50, 17953 (1994); (b) G. Kresse and D. Joubert, Phys. Rev. B 59, 1758 (1999).

[5] J. P. Perdew, K. Burke, and M. Ernzerhof, Phys. Rev. Lett. 77, 3865 (1996).

[6] (a) G. Kresse and J. Furthmuller, Comput. Mater. Sci. 6, 15 (1996); (b) G. Kresse and J. Furthmuller, Phys. Rev. B 54, 11169 (1996).

[7] P. Giannozzi, S. Baroni, N. Bonini, M. Calandra, R. Car, C. Cavazzoni, D. Ceresoli, G. L. Chiarotti, M. Cococcioni, I. Dabo et al., J. Phys.: Condens. Matter 21, 395502 (2009).

[8] G. J. Martyna, M. L. Klein and M. Tuckerman, J. Chem. Phys., 97, 2635 (1992).

[9] J. Nagamatsu, N. Nakagawa, T. Muranaka, Y. Zenitani, and J. Akimitsu, Nature (London) 410, 63 (2001).

[10] Y. Zhao, S. Zeng, and J. Ni, Phys. Rev. B 93, 014502 (2016).

[11] B. Y. Song, Y. Zhou, H. M. Yang, J. H. Liao, L.M. Yang, X. B. Yang, and E. Ganz, J. Am. Chem. Soc. 141, 3630 (2019).

[12] S. L. Bud'ko, G. Lapertot, C. Petrovic, C. E. Cunningham, N. Anderson, and P . C. Canfield, Phys. Rev. Lett. 86, 1877 (2001).